Design Power Control Strategies of Grid-Forming Inverters for Microgrid Application

Preprint

Jing Wang

National Renewable Energy Laboratory

Presented at the IEEE Energy Conversion Congress and Expo (ECCE 2021)
October 10–14, 2021

NREL is a national laboratory of the U.S. Department of Energy
Office of Energy Efficiency & Renewable Energy
Operated by the Alliance for Sustainable Energy, LLC

This report is available at no cost from the National Renewable Energy Laboratory (NREL) at www.nrel.gov/publications.

Contract No. DE-AC36-08GO28308

Conference Paper
NREL/CP-5D00-78874
October 2021

Design Power Control Strategies of Grid-Forming Inverters for Microgrid Application

Preprint

Jing Wang

National Renewable Energy Laboratory

Suggested Citation
Wang, Jing. 2021. *Design Power Control Strategies of Grid-Forming Inverters for Microgrid Application: Preprint*. Golden, CO: National Renewable Energy Laboratory. NREL/CP-5D00-78874. https://www.nrel.gov/docs/fy22osti/78874.pdf.

NREL is a national laboratory of the U.S. Department of Energy
Office of Energy Efficiency & Renewable Energy
Operated by the Alliance for Sustainable Energy, LLC

This report is available at no cost from the National Renewable Energy Laboratory (NREL) at www.nrel.gov/publications.

Contract No. DE-AC36-08GO28308

Conference Paper
NREL/CP-5D00-78874
October 2021

National Renewable Energy Laboratory
15013 Denver West Parkway
Golden, CO 80401
303-275-3000 • www.nrel.gov

NOTICE

This work was authored by the National Renewable Energy Laboratory, operated by Alliance for Sustainable Energy, LLC, for the U.S. Department of Energy (DOE) under Contract No. DE-AC36-08GO28308. Funding provided by U.S. Department of Energy Office of Electricity Delivery and Energy Reliability. The views expressed herein do not necessarily represent the views of the DOE or the U.S. Government.

Cover Photos by Dennis Schroeder: (clockwise, left to right) NREL 51934, NREL 45897, NREL 42160, NREL 45891, NREL 48097, NREL 46526.

NREL prints on paper that contains recycled content.

Design Power Control Strategies of Grid-Forming Inverters for Microgrid Application

Jing Wang
National Renewable Energy Laboratory, Golden, CO 80401, USA
jing.wang@nrel.gov

***Abstract*— This paper develops and compares two control schemes in the application control layer of a non-phase-locked loop (non-PLL) grid-forming (GFM) inverter to gain insight and understanding into how the two schemes affect the dynamic responses of GFM inverters and the transition operation of microgrids. The first scheme adopts power tracking based on an outer current loop in grid-connected mode and droop control in islanded mode, and the second uses droop control in both grid-connected and islanded modes. Analytical study is developed to compare the performance of these two strategies from various aspects, including fundamental differences, transition operation, power tracking, and P-Q capability with low point-of-common-coupling (PCC) voltages. Extensive simulation testing is carried out to validate the control performance of these two control strategies, and the simulation testing confirms the findings of the analytic study. Finally, the second strategy is recommended because of its superior control performance and ease of implementation. The analysis and results are useful in developing reliable control schemes for non-PLL GFM inverters because increasing numbers of inverters will work as non-PLL grid-forming sources in future grids because of their improved stability and reliability.**

Keywords—grid-forming inverter, power tracking, P-Q capability, smooth microgrid transition operation.

I. INTRODUCTION

Traditionally, inverter-interfaced distributed energy resources (DERs), such as photovoltaics (PV), have been designed as grid-following systems and need grid voltage/frequency to operate as the power injection source [1]. They cannot form the grid voltage, and they are required to trip off when the terminal voltage is not within the acceptable limits [2]. Because of the increasing penetrations of grid-connected DERs, it is necessary to redesign the functionalities of inverters to enable them to form the grid with their own voltages and frequencies, alleviate influences of harmful transients from the grid side, stay connected when needed, and avoid unnecessarily tripping off. These needs call for grid-forming (GFM) inverters, which will be critical assets in future electric grids. GFM inverters are grid-forming voltage sources without phase-locked loops (PLLs), and they can establish the system voltage and frequency during grid-connected and islanded modes. In this sense, the role of a GFM inverter is similar to the role of a synchronous generator [3]; therefore, synchronverter-type control is developed based on emulating the physics and dynamics of a synchronous generator to control a GFM inverter like a synchronous generator, such as in [4], [5].

Alternatively, emulating the operation of a synchronous generator is also a viable solution that allows the GFM inverter to behave like a synchronous generator with traditional double-loop control applied in the inverter control. For instance, [6] designed operation logics of startup, grid-connected, and islanded modes that mimic the operation of a real-world synchronous generator to synchronize a non-PLL GFM inverter to the grid, control the active and reactive power in grid-connected mode, and form system voltages in islanded mode. A double-loop voltage control with self-generated voltage and frequency was developed and validated with one GFM inverter in a microgrid application. This paper continues the effort developed in [6] to focus on designing control strategies in the application layer that generate the voltage references to achieve the selected control objective (e.g., power tracking and forming system voltages) based on the IEEE Std. 1676. The goal is to design the power tracking algorithm in the application layer that still allows the GFM inverter using its own voltage and frequency in grid-connected mode. Based on an extensive literature review, control strategies in the application layer can be classified into two categories: one category adopts power control based on a current control loop in grid-connected mode and droop control in islanded mode [7][8], and the second uses droop control for both grid-connected and islanded modes [9][10].

This paper develops the representative format of those two control schemes to ensure the stability and power tracking performance of GFM inverters and to achieve reliable and smooth microgrid transition operation. Further, an analytic study is performed to evaluate these two control strategies considering the fundamental differences, transition operation, power tracking performance, and P-Q capabilities under low point-of-common-coupling (PCC) voltages. Simulations are carried out to compare them in a microgrid with two non-PLL GFM inverters. Finally, recommendations are given based on the comparison of the control performance of these two control schemes.

The main contributions of this paper can be summarized as follows: 1) Two control strategies in the application layer are developed for GFM inverters to achieve power tracking in grid-connected mode and grid-forming in islanded mode; 2) An analytic study is developed to compare the performance of these two strategies from various aspects that are key for microgrid applications; 3) Comprehensive simulation testing is carried out to validate the control performance of these two control strategies, and the simulation testing confirms the results of the analytic study; and 4) Recommendations are given to one control strategy based on the superior control performance and ease of implementation. The analysis and results are useful in developing reliable control schemes for non-PLL GFM inverters because increasing numbers of inverters will work as non-PLL grid-forming sources in future grids because of their improved stability and reliability.

The remainder of this manuscript is organized as follows: The design of the control strategy of a non-PLL GFM inverter in the application layer is described in Section II. Two control schemes in the application layer are presented and analytic

comparisons are made in Section III. The simulations of a microgrid with two GFM inverters using two control schemes are presented in Section IV. The comparison of these two control strategies is summarized in Section V, and Section VI concludes the paper and gives the recommendation.

II. Control Strategy of Non-PLL GFM Inverters

Similar to a synchronous generator, a non-PLL GFM inverter generates its own frequency and voltage during both grid-connected and islanded modes without following the grid voltage. GFM inverters are controlled to inject a desired amount of active and reactive power into the grid when in grid-connected mode and to establish voltage and frequency in islanded mode. When applying IEEE Std. 1676, a voltage control scheme should be developed in the inverter control layer, and control schemes should be designed in the application control layer to track power references in grid-connected mode and to form grid voltages in islanded mode [7]. The recommended design practice is to use the same voltage control in the inverter control layer for both grid-connected and islanded modes, which ensures continuities in the state variables throughout the transition operation, thus achieving smooth transients during transition operation.

Table I. Operation Mode of GFM Inverter [6]

Start-up	Grid-Connected	Islanded
VF control	PQ control	VF control
S_1 open S_2 closed	S_1 closed S_2 closed	S_1 closed S_2 open
S_0 "0"	S_0 "1"	S_0 "0"
Internal V^* and ω^* references as nominal value	P^* and Q^*, externally configured and set by microgrid controller	*Internal* V^* and ω^*, references as nominal value

To synchronize a non-PLL GFM inverter to the grid, the GFM inverter runs in VF mode to start up and close the circuit breaker when its terminal voltage is synchronized with the grid voltage in terms of voltage magnitude, phase angle, and frequency. Table I summarizes the operation mode of a non-PLL GFM inverter emulating the operation of a synchronous generator in a microgrid application. Note that S_1 is the circuit breaker of the GFM inverter, and S_2 is the circuit breaker of the PCC of a microgrid. S_0 is the logic generated based on the status of S_1 and S_2, and it is used to switch between VF and PQ control based on the operation status of the GFM inverter. To achieve PQ control in grid-connected mode and VF control in islanded mode, the straightforward strategy is to switch between power tracking and voltage control, with both controls generating the voltage references for the inverter control layer. The frequency, ω, is held constant as the nominal frequency in grid-connected mode. In islanded mode, ω is dictated by the droop relationship in islanded mode because multiple GFM inverters could exist in the microgrid. This is the first control strategy in the application layer, called Strategy I. Because the droop control can be used to control the active and reactive power with control variables of frequency and voltage, the second control strategy, Strategy II, employs the same droop control for both grid-connected and islanded modes. Note that the active and reactive power references are zero in islanded mode because the goal is to control the voltage and frequency instead of power. These two control schemes in the application layer are presented in Fig. 1 (a) and Fig. 1 (b).

III. Compare Two Control Schemes in Application Layer for GFM Inverters

Fig. 1 (a) and Fig. (b) show the inverter main circuit, the control diagram of the inverter control layer, and the control schemes in the application control layer. Note that the control algorithm of the inverter control layer can be found in [7], which can control the inverter as an ideal voltage source. For both control schemes, active synchronization controls designed in [6] are applied during the inverter startup and microgrid reconnection to the grid to allow for the fast connection of a non-PLL GFM inverter and a microgrid to the grid. When there are multiple GFM inverters, only one GFM inverter—the one with the largest capacity—is assigned to perform the active synchronization control to reconnect the microgrid to the grid.

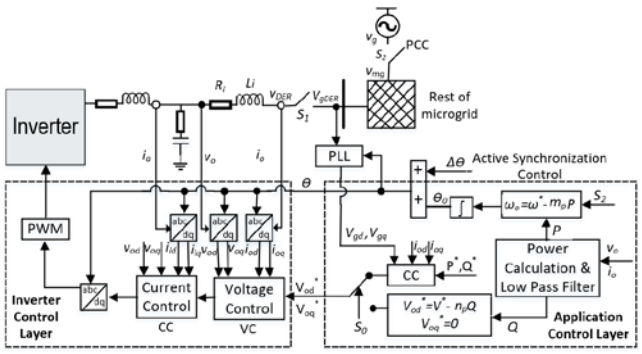

(a)

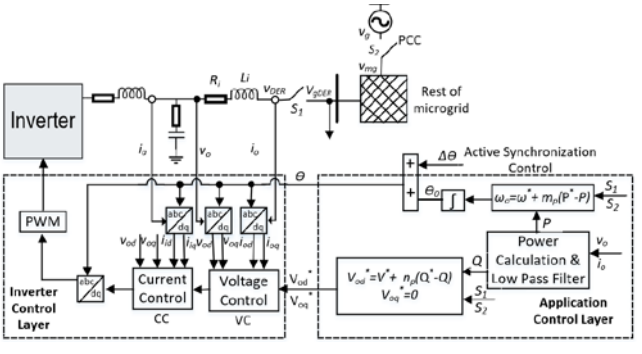

(b)

Fig. 1. Control diagram of the non-PLL GFM inverter in the inverter and the application control layer: (a) Strategy I and (b) Strategy II.

Table II outlines the control schemes in the application control layer and indicates that the only difference between the two schemes is in grid-connected mode.

Table II. Control Schemes in the Application Control Layer for the Two Control Strategies.

Control Strategy	Startup	Grid-Connected	Islanded
Strategy I	$\omega_o = \omega^*$ $V_{od}^* = V^*$ $V_{oq}^* = 0$	$\omega_o = \omega^*$ $V_{od}^* = V_{gd} + R_i i_{od}^* + K_{po}(i_{od}^* - i_{od}) - \omega_o L_i i_{oq}$, $i_{od}^* = \frac{2}{3}\frac{P^*}{V_{gd}}$ $V_{oq}^* = V_{gq} + R_i i_{oq}^* + K_{po}(i_{oq}^* - i_{oq}) + \omega_o L_i i_{od}$, $i_{oq}^* = -\frac{2}{3}\frac{Q^*}{V_{gd}}$	$\omega_o = \omega^* - m_p P$ $V_{od}^* = V^* - n_p Q$ $V_{oq}^* = 0$
Strategy II	$\omega_o = \omega^*$ $V_{od}^* = V^*$ $V_{oq}^* = 0$	$\omega_o = \omega^* + m_p(P^* - P) \rightarrow \omega_o = \omega^*, P^* = P$ $V_{od}^* = V^* + n_p(Q^* - Q) \rightarrow V_{od}^* = V^* + (n_p + \frac{k_{np}}{s})(Q^* - Q)$ $V_{oq}^* = 0$	$\omega_o = \omega^* - m_p P$ $V_{od}^* = V^* - n_p Q$ $V_{oq}^* = 0$

A. Fundamental Differences

Strategy I uses a model-based approach to generate the current reference and then to generate the voltage reference to track the active and reactive power. This loop in the application layer is known as an outer current loop.

In Strategy II, multiple GFM inverters must achieve the same frequency to reach system stability in steady state; this is the nominal frequency, ω^*. The actual frequency used in grid-connected mode is ω^*, and the active power tracking is accurate, with $P^* = P$. For reactive power tracking, a static tracking error always exists. Because the output impedances of the GFM inverters are different and because the line impedances between the GFM inverters are different, accurate reactive power sharing and tracking are impossible. This is a fundamental problem when using droop control for reactive power tracking. To achieve better reactive power tracking, an integrator is added to the droop equation to eliminate the static error, as shown in Table II. The gain of the integrator needs to be small so the dynamics of the voltage loop will not be significantly affected.

To study the differences between these two control schemes, the equivalent circuit of the inverter is shown in Fig. 2 (a), and a reduced-order small-signal model of this equivalent circuit is shown in Fig. 2 (b). The control algorithms of Strategy II follow these intrinsic power-angle dynamics in both grid-connected and islanded modes. When the microgrid transitions from one mode to another, there will be small step changes in the frequency ω and V_{od}^*; therefore, the dynamics of the voltage control in the inverter control layer shall be maintained relatively smooth because there is no need to switch between the references generated from grid-connected and islanded modes and V_{oq}^* is always equal to zero. For Strategy I, the control algorithm in grid-connected mode decouples the intrinsic power-angle characteristic shown in Fig. 2 (b). Alternatively, the relationship between the output power (P and Q) and the controlled voltage (V_o) is established based on the inverse dynamic model of the filter connected to the grid (R_i and L_i) in the synchronous frame for the power tracking, as shown in Fig. 2 (c). The outer current loop is used to generate the voltage reference, which contains feedback control and feed-forward elements. This control strategy in grid-connected mode introduces more transients and dynamics for the inverter layer control, especially when the grid voltage is involved. Further, this control strategy needs to switch between the voltage references generated in the application layer when the microgrid performs the transition operation, and larger changes in the voltage references are expected; therefore, GFM inverters may exhibit more transients when Strategy I is adopted.

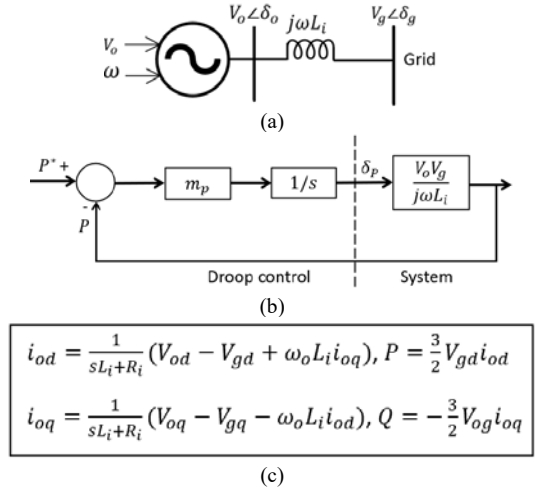

Fig. 2. Analytic study of the system: (a) equivalent model of the GFM inverter, (b) small-signal analysis of droop control [11], and (c) transfer function of the equivalent model in the synchronous frame.

B. Transition Operation

From grid-connected to islanded mode, the frequency of the GFM inverter changes from ω^* to $\omega^* - m_p P$ for both strategies, whereas the voltage references (v_{od}^*, v_{oq}^*) have step changes for Strategy I, and the voltage reference (v_{od}^*) has a small step change and v_{oq}^* has no change (equal to 0) for Strategy II. Thus, Strategy II shall have better transients during islanding operation.

As for the transition from islanded to grid-connected mode, the frequency of Strategy I changes from $\omega^* - m_p P$ to ω^*, and the frequency changes from $\omega^* - m_p P$ to $\omega^* + \Delta\omega$ for Strategy II. Thus, Strategy II is expected to experience more transients in frequency. Similar to islanding operation, the voltage references (v_{od}^*, v_{oq}^*) have step changes for Strategy I, and the voltage reference (v_{od}^*) has a small step change and v_{oq}^* has no change (equal to 0) for Strategy II during the reconnection operation. Note that the $\Delta\omega$ for Strategy II is generated because of the discrepancy between the target power and the actual power when the microgrid is reconnected. This $\Delta\omega$ will impact the power-angle stability and cause unwanted transients in frequency during reconnection. Only when the actual power tracks the power reference, this $\Delta\omega$ will be zero, and the system reaches steady state. Moreover, a proportional integral (PI) control is used in the reactive power tracking, which might cause transients and undershoot/overshoot in the output current of GFM inverters during reconnection. Hence, both strategies are expected to

have transients during reconnection, and Strategy I shall have better transients in the frequency and output power/current.

C. Power Tracking in Grid-Connected Mode

The power control loop for Strategy I is a current control loop that uses the inverse dynamic model of the L filter of the grid side to generate the voltage references for the inverter control layer. The grid voltage, v_{gDER}, is used as a reference to calculate the reference current, and it is also used as a feed-forward term in the current control loop to cancel the dynamics from the grid voltage. The synchronous frame elements of the grid voltage, v_{gd} and v_{gq}, are generated using the phase angle from the GFM inverter, instead of its own phase angle, to decouple the dependency with the grid dynamics. This is the source of the power tracking error because there is a pertinent phasor angle difference between the grid voltage (v_{gDER}) and the inverter voltage (v_o), and the dq components of the grid voltage (v_{gd}, v_{gq},) always deviate from the actual values (v'_{gd}, v'_{gq},) that are calculated by using its own PLL. Based on the mathematical calculation, v_{gd} is close to v'_{gd}, and v_{gq} is discrepant to v'_{gq} ($v'_{gq} = 0$); therefore, active power tracking performance might still be acceptable and has better tracking performance than the reactive power.

For Strategy II, the active power must track the active power reference to reach steady-state frequency for stability, and the reactive power can track the reactive power reference because of the PI control.

In terms of dynamics/transients, Strategy I should reach the reference without transients because of the inverse dynamic model approach, and Strategy II might exhibit some transients to settle down and reach steady state for both active and reactive power.

D. P-Q Capabilities Under Low PCC Voltages

Note that Strategy I uses grid voltage (v_{gDER}) to generate the voltage reference for power tracking in grid-connected mode, which indicates that the grid voltage (also called the PCC voltage) has an impact on the P-Q capability of the inverter if Strategy I is implemented. As for Strategy II, the PCC voltage also impacts its P-Q capability, but it is less obvious. In reality, a low PCC voltage caused by faults is common, and the fault ride-through capability of GFM inverters has become an important functionality requirement for improved system resilience [12]; therefore, we investigate the P-Q capability of the GFM inverter using both strategies under low-voltage conditions (0.5 and 0.2 p.u.). Following the P-Q capability calculation in [13], we obtained the P-Q capability curves shown in Fig. 3. Both figures show that Strategy II has a larger P-Q capability area than Strategy I under different low PCC voltages. The P-Q capability area of Strategy I decreases significantly with reduced PCC voltage. Especially for the PCC voltage with 0.2 p.u., the P-Q capability area is very small, which indicates possible instability when the PCC voltage reaches this low value.

Looking further at the equations listed in Table II, we can see that the power tracking of Strategy I in grid-connected mode depends on the PCC voltage; thus, the current references (i_{od}^*, i_{oq}^*) and voltage references (v_{od}^*, v_{oq}^*) can easily reach their limits when the PCC voltage is low. When the PCC voltage is very low (e.g., 0.2 p.u.), the system becomes unstable because of the saturation in each control loop. This limitation does not apply to Strategy II because there is no such dependency in the power control loop, and the low PCC voltage slightly impacts the frequency (ω) and the voltage reference (v_{od}^*). In islanded mode, these two strategies have the same P-Q capabilities because the algorithms are the same.

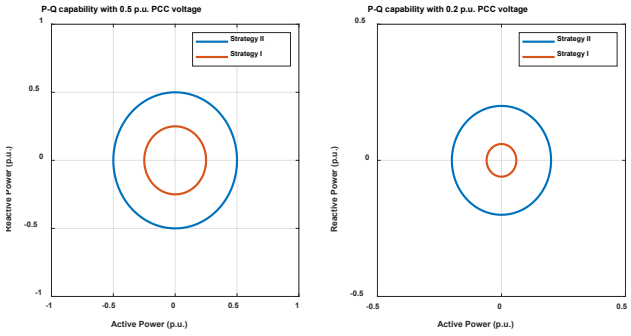

(a) (b)

Fig. 3. P-Q capability curve of the GFM inverter with different PCC voltages: (a) 0.5 p.u. PCC voltage and (b) 0.2 p.u. PCC voltage.

IV. Simulation Results

In this section, numerical simulations are performed in MATLAB/Simulink to validate the control performance of a non-PLL GFM inverter with the two control strategies presented in Section III. The microgrid system used for the simulation, which is described in [6], has two battery energy storage systems with inverters, two PV inverter units, and both residential and commercial buildings with load profiles. The two battery inverter systems are the GFM inverters in the system, and all other DERs (two PV units) are grid-following sources to inject power into the grid. Only the first battery is programed to perform active synchronization control when the microgrid is going to be reconnected to the main grid. The first GFM inverter is requested to connect to the grid at 1 s and the second at 1.5 s. To compare the control performance of these two strategies, a series of microgrid operations is performed, starting from grid-connected mode; then to unplanned islanding at 10 s; to islanded mode, with a plan for reconnection at 15 s; and finally to reconnection to the main grid. Representative results of each mode are selected and illustrated.

Full Simulation Scenario: Fig. 4 shows the key measurements of the microgrid with two control strategies, including PCC circuit breaker status (top trace), PCC voltage root mean square (RMS) in per unit (middle), and frequency (bottom). The results show that the PCC voltages are similar for the two control strategies, and the frequency shows a smoother transient with Strategy II during islanding operation and a superior transient with Strategy I during reconnection operation. Note that the transients shown at t=15 s are caused by the active synchronization control, which adds the angle difference between the main grid and the microgrid in the first GFM inverter to accelerate the reconnection process. Both strategies achieve smooth and successful microgrid transition operation.

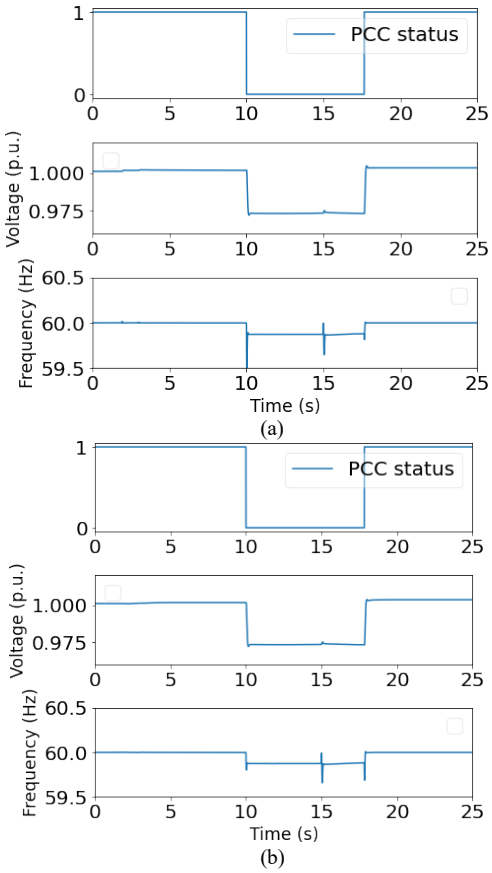

Fig. 4. Results of the full simulation scenario: PCC circuit breaker status, PCC voltage RMS and frequency: (a) Strategy I and (b) Strategy II.

Unplanned Islanding Operation: Test results of the microgrid unplanned islanding (t=10 s) for the two strategies are presented in Fig. 5 (a) and Fig. 5 (b). The results include the phase angle, output voltage, and current of two GFM inverters. As shown, the phase angle of the GFM inverters stays continuous and smooth, without a phase jump, for both strategies because of the self-generated frequency of the GFM inverters during both grid-connected and islanded modes. Further, the zoomed-in pictures of the output voltage and the current of the GFM inverters during unplanned islanding operation indicate very smooth transients for both strategies. The output currents of both GFM inverters with Strategy II have less distortion than those with Strategy I. A closer look at the phase angle, output voltage, and current of the GFM inverters for the two strategies shows that they are almost the same for both strategies even though the control strategies are different in grid-connected mode.

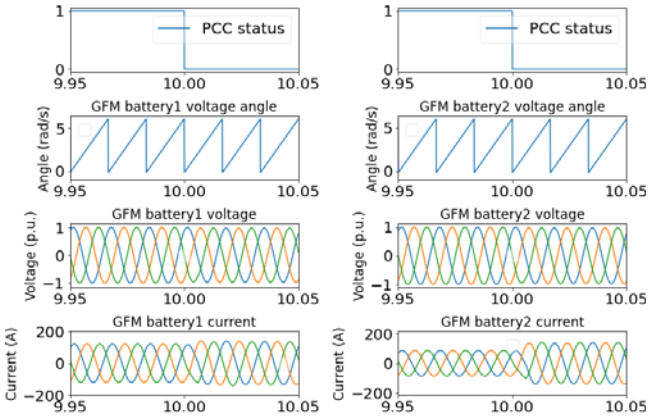

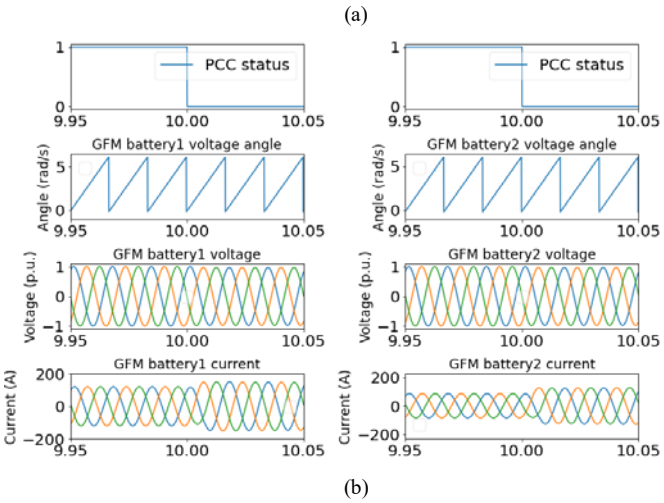

Fig. 5. Key results in the unplanned islanding operation: (a) Strategy I and (b) Strategy II.

Reconnection Operation: The test results of the microgrid reconnection (started at t=15 s) for the two strategies are shown in Fig. 6 (a) and Fig. 6 (b). Note that the microgrid reconnects to the main grid at t=17.646 s with Strategy I and at t=17.834 s with Strategy II, and the same reconnection criteria are applied at the PCC circuit breaker control. Both strategies have smooth transients in the phase angle and the output voltage of the GFM inverters during reconnection operation. The output currents of the two GFM inverters exhibit distortions for Strategy I and relatively fewer distortions for Strategy II. The output currents of the GFM inverters in a relatively longer timescale are presented in Fig. 6, which shows that the output currents in Strategy I reach steady state rapidly within a few cycles, and the output currents have overshoots and reach steady state slower in Strategy II. The distortions observed in the output currents of the two GFM inverters for Strategy I are caused by the inverse dynamic model in the outer current loop and the switch between voltage references as well as the fast setting time thanks to the inverse dynamic model for fast tracking capability. The frequency (ω_o), active and reactive power of the two GFM inverters for both strategies are presented in Fig. 6 (a) and Fig. 6 (b), respectively. These results confirm those of the analytic study in Section III in that the frequencies of the GFM inverters using Strategy II experience transients because of the discrepancy between the target power and the measured power, and they settle down only when the active power reaches the target values. The responses of the reactive power are caused by the PI control, and the output active and reactive power of the two GFM inverters reach steady state in 0.6 s. Compared to Strategy II, the frequencies in Strategy I have no transient, and the output active and reactive power exhibit small oscillations and reach steady state in less than 0.05 s. Overall, Strategy I has better transients in system frequency and output power/current.

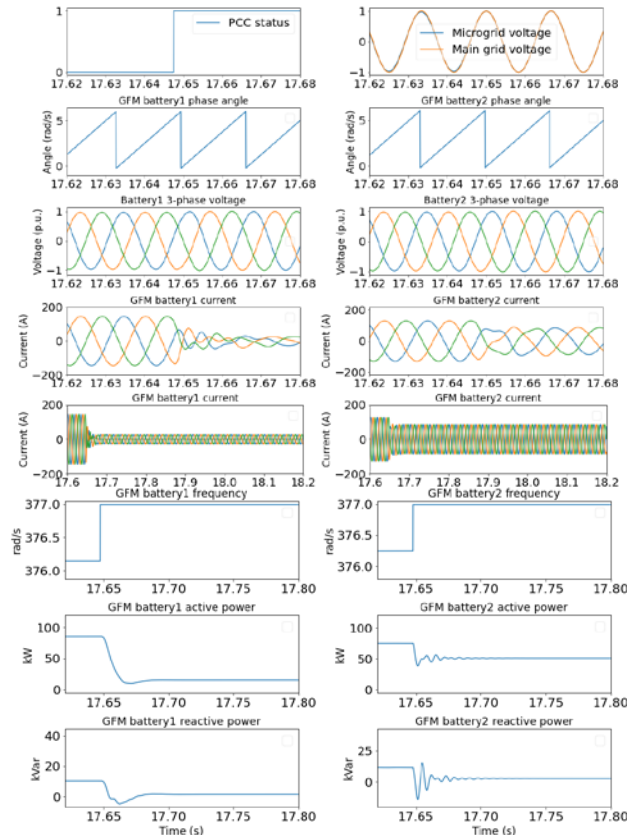

(a)

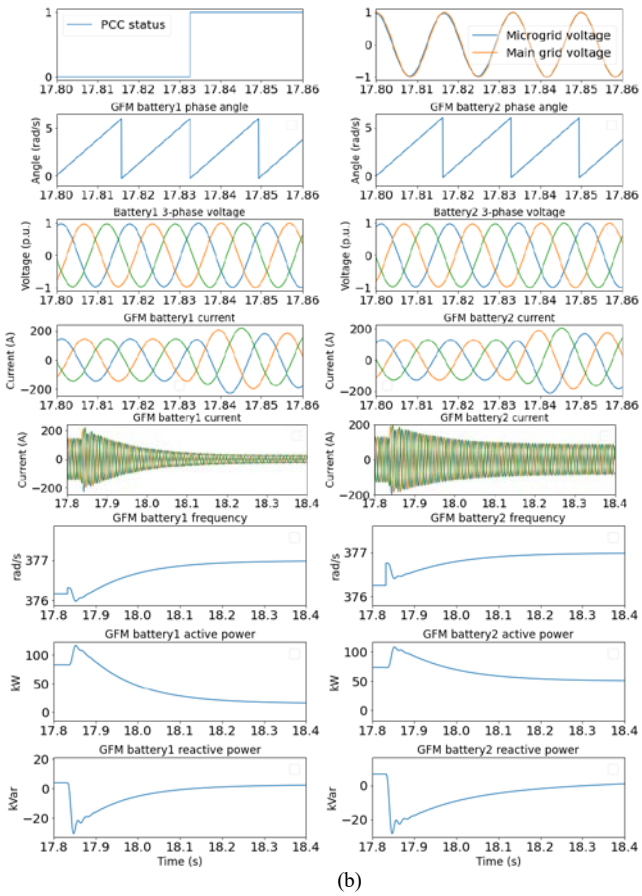

(b)

Fig. 6. Key results in the reconnection operation: (a) Strategy I and (b) Strategy II.

Power Tracking Performance in Grid-Connected Mode: To compare the power tracking performance of two control strategies, the active and reactive power references are changed multiple times in grid-connected mode. Only the results of the first GFM inverter are presented and shown in Fig. 7. The results show that the active power output of Strategy I follows the reference tightly without settling time thanks to the control based on the inverse dynamic model. Similar dynamics are observed with the reactive power; however, there is a static tracking error. This is caused by the inaccurate current references (i_{od}^*, i_{oq}^*), which should be generated using the phase angle of the grid voltage, V_{gDER}, instead of the voltage angle of the inverter, V_o. Note that when the reactive power reference is small, the errors of the current references are relatively small as well. So, the reactive power can track the reference better. For Strategy II, both active and reactive power track the reference within an acceptable settling time (approximately 0.5 s). The active power tracking is achieved because the GFM inverter must reach the frequency, ω_o, in steady state, and the active power output is naturally bounded to generate power equal to the reference power to achieve that. For the reactive power, the integrator is essential to cancel out the tracking error.

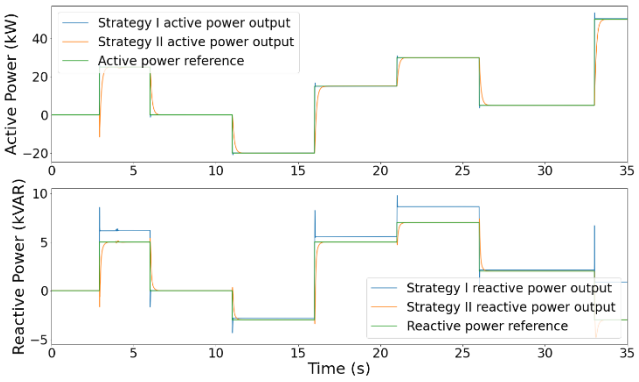

Fig. 7. Power tracking of the first GFM battery inverter for two control strategies: active power (top) and reactive power (bottom).

P-Q Capability with Low PCC Voltages in Grid-Connected Mode: Three-phase-to-ground-faults are added to create low PCC voltages and to compare the robustness and P-Q capability of the two control strategies in grid-connected mode. The three-phase-to-ground faults are added as follows: 1) A fault with 5 Ω impedance is triggered at 6 s and removed at 6.05 s; 2) A fault with 0.5 Ω fault impedance is trigged at 12 s and removed at 12.05 s; and 3) A fault with 0.05 Ω fault impedance is triggered at 16 s and removed at 16.05 s. The first fault reduces the PCC voltage to approximately 0.5 p.u., and the second and third faults reduce the PCC voltages even further, to near 0.2 p.u. For a fair comparison, the active and reactive power set points for the first GFM inverter are constant during the whole test, with 150 kW (0.425 p.u.) and 5 kVar (0.0142 p.u.), respectively. Faults are added to the same bus that connects the first GFM inverters. The representative results of the first GFM inverter for both control strategies are presented in Fig. 8 through Fig. 10.

Fig. 8 shows the three-phase voltage of the GFM inverter of the two strategies under three different fault conditions. For Strategy I, the GFM inverter maintains voltage stability for the first fault condition, with a PCC voltage of 0.5 p.u.; and it lost stability with the second and the third fault conditions, with PCC voltages of 0.2 p.u. For Strategy II, the GFM inverter maintains voltage stability for the three fault

conditions. The results mean that the inverter with Strategy I has sufficient P-Q capability for the first fault condition, but the P-Q capability is not enough for the second and the third fault conditions. In contrast, the inverter with Strategy II has sufficient P-Q capability for all three fault conditions. These results align with the analytic study that shows that Strategy I has a very small P-Q capability with a very low PCC voltage (0.2 p.u.).

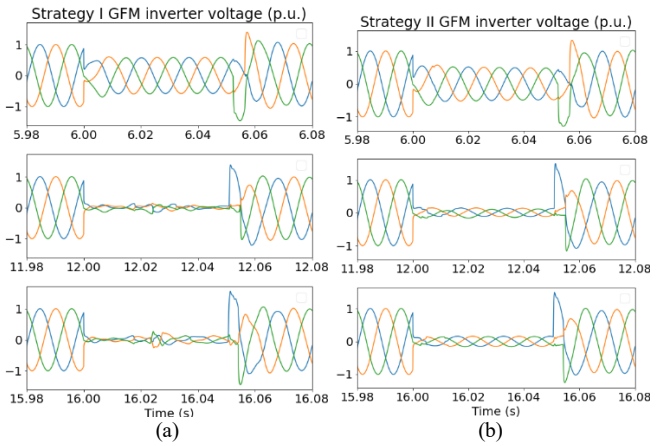

(a) (b)

Fig. 8. Three-phase voltage of the GFM inverter under three different fault conditions: (a) Strategy I and (b) Strategy II.

Fig. 9 shows the three-phase output current of the GFM inverter of two strategies under three different fault conditions. Similar to the results shown in Fig. 8, Strategy I can maintain current stability for the first fault condition but loses its current stability for the second and the third fault conditions. For Strategy II, the current in the fault condition is close to its nominal value, and it is slighlty higher than 1 p.u. for the second and third fualt conditions. Further, it can maintain current stability with all three fault conditions.

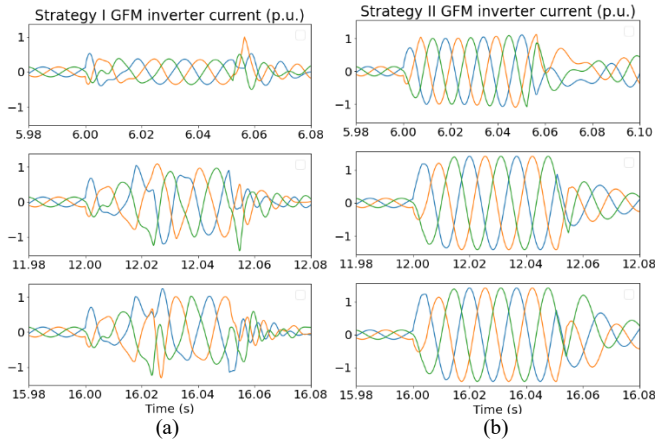

(a) (b)

Fig. 9. Three-phase current of the GFM inverter under three different fault conditions: (a) Strategy I and (b) Strategy II.

A further look at the voltage dq components better shows how the PCC voltage impacts the two control strategies. Fig. 10 (a) shows the voltage dq components for Strategy I, which indicates large spikes (more than 2 p.u.) in both dq components under the fault conditions, especially for the third fault. Again, the voltage references are generated based on the current control in the power loop, which experiences large spikes because the current references depend on the PCC voltage. For Strategy II, there are spikes for each fault condition; however, the magnitudes of the dq components at each fault are smaller and accepable. Even though the same voltage control algorithm is used for both strategies, a different control strategy in the power loop still has a big impact on the stability and P-Q capability of the GFM inverter. The results under this test scenario illustrate that Strategy II has better robustness than Strategy I under the three-phase fault conditions with low PCC voltages.

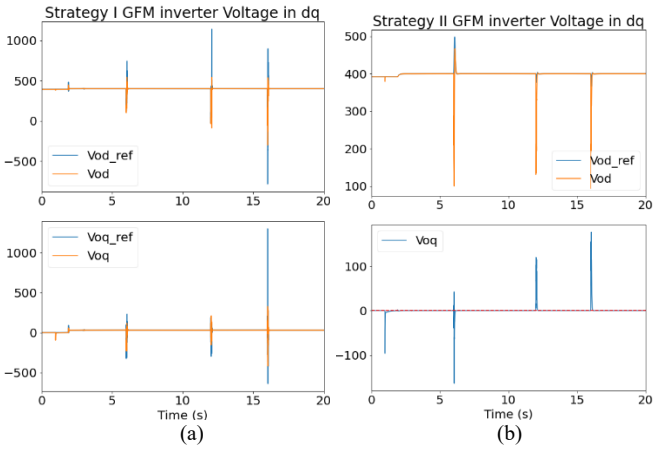

(a) (b)

Fig. 10. dq components of the GFM inverter voltage under three different fault conditions: (a) Strategy I and (b) Strategy II.

V. Discussion

Based on the analytic study and simulation results, Table III summarizes the performance of the GFM inverter with the two strategies.

Table III Summary of the Performance.

Circumstance	Strategy Comparison
Unplanned islanding	Both have smooth transients. Strategy II has slightly better transients in the output current.
Reconnection operation	Strategy I has better transients in frequency, output current, and power.
Power tracking	Strategy I reaches steady state faster with overshoots and has a tracking error in the reactive power. Strategy II has good tracking performance for both active and reactive power with an acceptable settling time.
P-Q capability with low PCC voltage	The low PCC voltage has a larger impact for Strategy I because its power control loop is a current control loop, and the current references depend on the PCC voltage. Strategy II has a larger P-Q capability with low PCC voltages and can maintain stability during fault ride-through. Strategy I can maintain stability only when the voltage is not less than a certain level.

Strategy II overperforms Strategy I because it has better power tracking performance and a larger P-Q capability for fault ride-through, and its transients during islanding and reconnection operations are comparable to Strategy I. Further, Strategy II is easier to implement, and the power control loop can maintain the same control structure in both grid-connected and islanded modes; therefore, Strategy II is recommended for microgrid applications. If Strategy II is implemented, the PI control parameters of the reactive power droop need to be cautiously tuned to maintain stability and

the expected transients under various dynamic events and operations.

VI. Conclusion

This paper presents two control schemes in the application layer of a non-PLL GFM inverter for microgrid applications. The first control scheme uses a current-control loop for power tracking in grid-connected mode and droop control in islanded mode, and the second scheme adopts droop control in both grid-connected and islanded modes. The first scheme is expected to exhibit more transients during transition operation because of relatively large step changes in the voltage references and the inverse dynamic model-based control in grid-connected mode. The power tracking error during reconnection affects the power angle stability of the second scheme, which is expected to have more transients during reconnection. A microgrid with two GFM inverters is tested under full operation, including grid-connected mode, unplanned islanding, islanded mode, and reconnection to the grid. Simulation results show that both control schemes achieve successful transition operation with smooth transients—the second control scheme exhibits slightly better transients in system frequency and the output current of the GFM inverters during islanding operation, and the first control scheme has slightly superior transients in system frequency and the output power of the GFM inverters during reconnection operation. These results confirm those of the analytic study.

Additional tests, including power tracking in grid-connected mode and fault ride-through, are performed to further compare these two control strategies. Strategy II exhibits superior power tracking performance and a larger P-Q capability in the fault ride-through with different fault conditions. Overall, Strategy II is recommended for microgrid applications because of its comparable transition operation performance, better power tracking and P-Q capability under faults, and its ease of implementation.

Acknowledgments

This work was authored by the National Renewable Energy Laboratory, operated by Alliance for Sustainable Energy, LLC, for the U.S. Department of Energy (DOE) under Contract No. DE-AC36-08GO28308. Funding provided by U.S. Department of Energy Office of Electricity Delivery and Energy Reliability. The views expressed in the article do not necessarily represent the views of the DOE or the U.S. Government. The U.S. Government retains and the publisher, by accepting the article for publication, acknowledges that the U.S. Government retains a nonexclusive, paid-up, irrevocable, worldwide license to publish or reproduce the published form of this work, or allow others to do so, for U.S. Government purposes.

References

[1] Joan Rocabert, Alvaro Luna, Frede Blaabjerg, Pedro Rodriguez, "Control of Power Converters in AC Microgrids", *IEEE Trans. Power Electron.*, vol. 27, no. 11, pp. 4734-4749, Nov. 2012.

[2] IEEE Std 1547, IEEE Standard for Interconnecting Distributed Resources with Electric Power Systems.

[3] B. Mahamedi and J. Fletcher, "The Equivalent Models of Grid-Forming Inverters in the Sequence Domain for the Steady-State Analysis of Power Systems," *IEEE Tran. Power Systems*, vol. 35, no. 4, July 2020, pp. 2876-2887.

[4] Q. Zhong and G. Weiss, "Synchronverters: Inverters That Mimic Synchronous Generators," *IEEE Tran. Ind. Electron.*, vol. 58, no. 4, April 2011, pp. 1259-1267.

[5] Qingchang Zhong, "Virtual Synchronous Machines: A Unified Interface for Grid Integration," *IEEE Power Electronics Magazine*, vol. 3, issue. 4, Dec. 2016, pp. 18-27.

[6] J. Wang, B. Lundstrom and A. Berinstein, "Design of a Non-PLL Grid-Forming Inverter for Smooth Microgrid Transition Operation," *IEEE Power & Energy Soceity General Meeting (PESGM) 2020*, Montral, Canada, 2-6 Aug. 2020.

[7] J. Wang, et al., "Design of a Generalized Control Algorithm for Parallel Inverers for Smooth Microgrid Transition Operaiton," *IEEE Ind. Electron.*, vol 62, no. 8, August 2015, pp. 4900-4914.

[8] J. Wang, et al., "Design of an advanced energy management system for microgrid control using a state machine," *Applied Energy*, volume 228, Oct. 2018, pp. 2407-2421.

[9] J. M. Guerrero, et al., "Hierarchical Control of Droop-Controlled AC and DC Microgrids-A General Approach Towards Standardization," *IEEE Tran. Ind. Electron*., vol. 58, no. 1., Jan. 2011, pp. 158-172.

[10] J. M. Guerrero, et al., "Advanced Control Architectures for Intelligent Microgrids-Part I: Decentralizd and Hierarchical Control," IEEE *Tran. Ind. Electron*., vol. 60, no. 4, April 2013, pp. 1254-1262.

[11] W. Du, et al., "A Comparative Study of Two Widely Used Grid-Forming Droop Controls on Microgrid Small-Signal Stability," *IEEE Journal of Emerging and Selected Topics in Power Electronics*, vol. 8, no. 2, June 2020, pp. 963-975.

[12] Research Roadmap on Grid-Forming Inverters. Y. Lin et al. Available: https://www.nrel.gov/docs/fy21osti/73476.pdf.

[13] B. Lu, et al., "Dynamic P-Q Capability and Abnormal Operation Analysis of Inverter Based Resources," *IEEE Journal of Emerging and Selected Topics in Power Electronics* (under review).